# Comparison of subspace identification methods for modal estimation of bladed disks

Corentin Jorajuria, Cécile Esteves, Claude Gibert, Fabrice Thouverez

# Comparison of subspace identification methods for modal estimation of bladed disks

Corentin Jorajuria[a,*], Cécile Esteves[b], Claude Gibert[a], Fabrice Thouverez[a]

[a] *Ecole Centrale de Lyon, CNRS, ENTPE, Laboratoire de Tribologie et Dynamique des Systèmes, UMR5513, 69130 Ecully, France*
[b] *Safran Aircraft Engines, 77550 Moissy-Cramayel, France*

**Abstract**

Bladed disks are critical parts of aeronautic turbojet engines requiring numerous dynamic analysis tests to fully achieve their design process. This work presents subspace state-space identification techniques for estimation of modal parameters of bladed disks using realistic although numerically generated test case data. Indeed, modal testing of bladed disks can exhibit high modal density leading to modal estimation issues. This study focuses on subspace state-space identification framework as it is an efficient way to process vector-valued time series and thus to estimate modal parameters in a context of high modal density. In order to evaluate the techniques of interest, a versatile modal model has been specifically implemented to simulate data representative of full-scale rotating aeronautic fan modal tests. This model is easily adjustable allowing to evaluate the identification methods in a more or less severe estimation context. The performance of the investigated methods are discussed and compared with the prescribed parameters of the model. Moreover, different techniques to estimate the order of the associated state-space model are reviewed and tested over several simulated configurations. Finally, a method to evaluate the uncertainties over the modal parameters using covariance of estimator results and pseudospectrum computation is proposed and discussed over the investigated test cases.

*Keywords:* modal testing, subspace identification, state-space representation, bladed disks, aeronautic turbojet engines, uncertainties estimation.

## Introduction

Comprehension of energy dissipation phenomena is a crucial challenge in rotor dynamics. As these phenomena are very wide and complex, experimental studies play an important role to quantify damping. A recent publication has proposed a method to estimate modal parameters without requiring resonance crossing using time-frequency representation [1]. This technique has been applied on steam turbine and tackles several challenges, among which the identification of closed-space modes requiring high frequency resolution not often possible in operational conditions. Closed-space modes estimation issue has also been put forward for composite aeronautic fan, this time using piezoelectric induced stepped sine excitations and frequency domain identification methods [2]. Among the time estimation methods [3], subspace state-space identification techniques are particularly attractive to meet high modal density identification challenges as they propose to identify minimal statistics of multivariate time series. This article focuses on comparing different subspace state-space identification methods. First section presents general concepts for time identification and describes two subspace state-space methods. Second section briefly addresses the problem of order determination. Third section focuses on estimation of uncertainties in state-space representation and how to propagate these uncertainties to modal parameters. Last section deals with application by means of a versatile yet

*Corresponding author
*Email address:* corentin.jorajuria@ec-lyon.fr (Corentin Jorajuria)

representative model of a bladed disk allowing to evaluate the performances of the presented identification methods. Useful symbols and abbreviations have been summed up at the end of this article.

## 1. Subspace identification methods

### *1.1. Time series identification*

This section briefly presents prediction theory framework and state-space representation, two concepts useful for subspace state-space identification methods.

The prediction theory framework [4] formalizes the identification of system dynamics from experimental observations. It relies on the principle that to identify a causal system is equivalent to predict the future dynamics knowing its past dynamics. The following of the study considers system dynamics observed through $n_o$ discrete time signals. In this context, the prediction theory framework proposes to predict the more likely realization of the future of the observations $y_{t+\tau} \in \mathbb{R}^{n_o}$ at time $t$ with $\tau > 0$ among the possible linear combinations of $y_t$ components. The restriction of the solution to this vector space, denoted $\mathcal{S}_t$, is particularly pertinent for linear systems (cf. [4]).

$$\mathcal{S}_t = \left\{ \zeta_t = \sum_{k=0}^{n_\zeta} G_k y_{t-k} \;\middle|\; G_k \in \mathbb{R}^{n_o \times n_o},\ n_\zeta \in \mathbb{N} \right\}$$

The synthesized observations $\zeta_t$ are the vector elements and the coefficients $G_{ij,k}$ are the coordinates in the canonical basis. Mathematical notation $G_{ij,k}$ denotes coefficient of row $i$ and column $j$ of matrix $G_k$. Assuming observations are weakly stationary stochastic processes of order two, one can build a scalar product from the bilinear operator over column vectors $(a, b) \mapsto \mathbb{E}[a^T b]$. In explicit terms, consider $\zeta_t,\ \eta_t$ in $\mathcal{S}_t$ having respectively coordinates $G_{ij,k},\ E_{ij,k}$ in the canonical basis.

$$\langle \eta_t, \zeta_t \rangle = \sum_{k,l=0}^{n_\zeta, n_\eta} \mathbb{E}\left[ y_{t-l}^T E_l^T G_k y_{t-k} \right] = \sum_{k,l=0}^{n_\zeta, n_\eta} \operatorname{trace}\left( G_k \Gamma_{yy(k-l)} E_l^T \right) \tag{1a}$$

$$\|\zeta_t\| = \sqrt{\langle \zeta_t, \zeta_t \rangle} \tag{1b}$$

The autocorrelation function of the weakly stationary observations $\Gamma_{yy(k-l)} = \mathbb{E}\left[ y_{t-k} y_{t-l}^T \right]$ has been introduced in the above equations. Using the norm in equation (1b), the vector space of linear combinations of $y_t$ can be completed to a Hilbert space, denoted $\mathcal{H}$. The restriction to the subspace generated by the past observations is denoted $\mathcal{Y}_t$.

$$\mathcal{H} = \left\{ \zeta_t = \sum_{k=-\infty}^{+\infty} G_k y_{t-k} \;\middle|\; G_k \in \mathbb{R}^{n_o \times n_o},\ \sum_{k=-\infty}^{+\infty} \|G_k\|_{\mathrm{F}}^2 < +\infty \right\}$$

$$\mathcal{Y}_t = \left\{ \zeta_t = \sum_{k=0}^{+\infty} G_k y_{t-k} \;\middle|\; G_k \in \mathbb{R}^{n_o \times n_o},\ \sum_{k=0}^{+\infty} \|G_k\|_{\mathrm{F}}^2 < +\infty \right\}$$

Where $\|.\|_{\mathrm{F}}$ is the Frobenius norm. The prediction theory framework consists in finding, at time $t$, $\hat{y}_{t+\tau}$ the element of $\mathcal{Y}_t$ closest to $y_{t+\tau}$. In prediction theory, the identification criterion often requires minimizing the variance of the error. This is equivalent to choose as estimate the closest element in the sense of the norm defined in equation (1b). This is why, in prediction theory, the minimum variance estimate is often presented as the orthogonal projection of the future observations onto the subspace generated by the past observations. For random variable of $L^2$, the minimum variance estimate coincides with the conditional expectation.

State-space representations are useful to process multivariate time series as they provide compact models for system dynamics. The presented identification techniques assume linear time invariant systems with

finite order $n$. State-space representations can be expressed in "Process" form using the state-space matrices, the states $x_t$, and the zero-mean perturbation processes $w_t$ and $v_t$.

$$\begin{aligned} x_{t+1} &= Ax_t + Bu_t + w_t \\ y_t &= Cx_t + Du_t + Sw_t + v_t \\ \text{with} \quad \mathbb{E}\left[w_t w_s^T\right] &= Q\delta_{ts}, \ \ \mathbb{E}\left[v_t v_s^T\right] = R\delta_{ts} \ \text{ and } \ \mathbb{E}\left[w_t v_s^T\right] = 0 \end{aligned} \tag{2}$$

Where $y_t \in \mathbb{R}^{n_o}$ is the observation vector at a given time $t$, and $u_t \in \mathbb{R}^{n_i}$ is the excitation vector. The matrices $A, B, C, D$ are respectively the transition, control, observation and feed-forward matrices. The states vector $x_t \in \mathbb{R}^n$ gives minimal statistics to describe the system dynamics. The perturbation process on states transition, $w$, represents the error over states vector estimate while the perturbation on system observation, $v$, depicts the observation error. The two perturbation processes $w$ and $v$ are assumed independent one to another, uncorrelated in time, Gaussian, and have covariance matrices $Q$ and $R$ respectively. Also, $w_t$ and $v_t$ are assumed to be independent of $x_t$ and $u_t$. The matrix $S$ models the contribution of the system noise in the observation equation. To identify subspace using prediction theory framework the system equation (2) is considered over finite time recursion $h$, called "horizon", leading to the following stacked vector equation.

$$y_{t|h} = \mathcal{O}_h x_t + \Psi_h u_{t|h} + \Gamma_h w_{t|h} + v_{t|h} \tag{3}$$

$$\text{with, } \mathcal{O}_h = \begin{bmatrix} C \\ CA \\ \vdots \\ CA^{h-1} \end{bmatrix} \qquad m_{t|h} = \begin{bmatrix} m_t \\ m_{t+1} \\ \vdots \\ m_{t+h-1} \end{bmatrix} \quad \text{for } m = y, u, w, v$$

$$\Psi_h = \begin{bmatrix} D & 0 & \dots & 0 \\ CB & D & \dots & 0 \\ \vdots & \vdots & \ddots & \vdots \\ CA^{h-2}B & CA^{h-3}B & \dots & D \end{bmatrix} \qquad \Gamma_h = \begin{bmatrix} S & 0 & \dots & 0 \\ C & S & \dots & 0 \\ \vdots & \vdots & \ddots & \vdots \\ CA^{h-2} & CA^{h-3} & \dots & S \end{bmatrix}$$

Where $\mathcal{O}_h$ represents the extended observability matrix. In control theory, a system of order $n$ is described as observable when the observability matrix $\mathcal{O}_n$ is of rank $n$, formalizing the concept that all the states can be observed by means of the measured data.

### *1.2. Minimum variance criterion*

A natural choice to estimate the system dynamics consists in minimizing the error between predicted and measured dynamics. Using the norm presented in the above section, this choice leads to minimizing the covariance error matrix.

The Multi-Output Error State space (MOESP) identification technique was proposed in 1991 [5]. It tackles identification of multivariate finite order systems with error in the output signals using a state-space representation. The main advantage is to propose a compact and efficient identification algorithm consisting in a pre-processing of signals into "data matrices", a LQ decomposition followed by a singular value decomposition and finally the resolution of an overdetermined matrix equation. Series of identification techniques relying on this algorithmic structure have then been proposed to improve this identification framework. Several variants with and without the use of instrumental variable method has been proposed "elementary MOESP", "ordinary MOESP", "MOESP-PI", "MOESP-RS" [6–8] and "MOESP-PO" [9].

Numerical algorithms for Subspace State Space System Identification (N4SID), proposed by P. Van Overschee and B. de Moor [10–12], extends the MOESP techniques to a more general and efficient framework. N4SID framework proposes two algorithms to estimate the state-space matrices, one using observability estimation, the other using states estimation. Moreover, this framework has been extended to cover other identification strategies including the canonical variate analysis [13]. For the numerical tests we have retained only one of the identification techniques with a criterion based on minimum variance: N4SID with MOESP weighting. This algorithm is equivalent to MOESP with instrumental variable "PO" (cf. [9]).

The first step of all N4SID algorithms consists in pre-processing the experiment data $y_t$ and $u_t$ to build

structured matrices. These matrices are organized as follows:

$$M_{t|h,N} = \begin{bmatrix} m_t & m_{t+1} & \dots & m_{t+N-1} \\ m_{t+1} & m_{t+2} & \dots & m_{t+N} \\ \vdots & \vdots & \ddots & \vdots \\ m_{t+h-1} & m_{t+h} & \dots & m_{t+h+N-2} \end{bmatrix} \in \mathbb{R}^{\dim(m)h \times N}$$
with $m = y, u, w, v$.

The triplet $(t, h, N)$ determines the signal samples stored in $M_{t|h,N}$ as well as the dimension of these matrices. The orders of time shift $h$ and $N$ are respectively the horizon and the number of temporal samples used to estimate the statistical expectation empirically. Indeed, using the ergodicity assumption, the estimate of the expectation of a product comes down to a row matrix multiplication scaled by $N$:

$$\begin{aligned} \mathbb{E}\left[\rho_t^T m_t\right] &= \frac{1}{N}\sum_{k=0}^{N-1} \rho_{t+k}^T m_{t+k} + O(\epsilon_N) \\ &= \frac{1}{N}\text{trace}\left(\wp_{t|1,N}{}^T M_{t|1,N}\right) + O(\epsilon_N) \\ &\text{with} \quad M_{t|1,N} = \begin{bmatrix} m_t & m_{t+1} & \dots & m_{t+N-1} \end{bmatrix}, \\ &\qquad \wp_{t|1,N} = \begin{bmatrix} \rho_t & \rho_{t+1} & \dots & \rho_{t+N-1} \end{bmatrix}, \\ &\qquad \text{and} \ \lim_{N\to\infty} \epsilon_N = 0. \end{aligned}$$

Ergodicity assumption gives $O(\epsilon_N) \approx 0$. The dimension $N$ can be taken such as verifying $\dim(m) \cdot h \ll N$, in such cases data matrix $M_{t|h,N}$ is said to be wide rectangular. In the prediction theory framework, the row vector $Y_{t|1,N}$ interprets a finite sampling of the signal $y_t$ and the combination of rows of the matrix $Y_{t|h,N}$ interprets the subspace generated by the sampled signal over a horizon $h$. The stacked vector equation (3) gives the following equation for the data matrices:

$$Y_{t|h,N} = \mathcal{O}_h X_{t|1,N} + \Psi_h U_{t|h,N} + \Gamma_h W_{t|h,N} + V_{t|h,N}. \tag{4}$$

N4SID proposes to split the system dynamics in two, a "past" and "future" dynamics, and to identify the subspace of future states using input information data and past observations. In order to make better use of past and future concepts, we introduce $M_p = M_{t|h,N}$ for past data matrix and $M_f = M_{t+h|h,N}$ for future data matrix. Then the following matrix equations hold:

$$X_f = A^h X_p + \mathcal{C}'_h U_p + \mathcal{F}'_h W_p \tag{5a}$$

$$Y_f = \mathcal{O}_h X_f + \Psi_h U_f + \Gamma_h W_f + V_f \tag{5b}$$

$$\text{with} \quad \mathcal{C}'_h = [A^{h-1}B \ \dots \ AB \ B] \quad \mathcal{F}'_h = [A^{h-1} \ \dots \ A \ I].$$

Where the reversed extended reachability matrix has been introduced $\mathcal{C}'_h$. Equation (5a) describes states transition between the past and future states matrices and equation (5b) corresponds to the observation equation for future data matrices. As $v_t$ and $w_t$ are assumed independent of $x_t$ and $u_t$ equation (5b) can be written as follows:

$$Y_f = \mathcal{O}_h X_f + \Psi_h U_f + V'_f \tag{6}$$

$$\text{with} \quad V'_f = \Gamma_h W_f + V_f, \quad \tfrac{1}{N} X_f V'^T_f = 0 \quad \text{and} \quad \tfrac{1}{N} U_f V'^T_f = 0.$$

The above formulation will be useful to identify $\mathcal{O}_h X_f$ from known matrices $Y_f$ and $U_f$.

The next step consists in performing the LQ decomposition of the full data matrix $H$ (cf. equation 7). The LQ decomposition provides an efficient data compression along with a useful decomposition for subspace identification. This decomposition corresponds to the Gram-Schmidt orthogonalization process for a matrix interpreted as a stack of row vectors.

$$H = \begin{bmatrix} U_f \\ U_p \\ Y_p \\ Y_f \end{bmatrix} = \begin{bmatrix} U_f \\ Z_p \\ Y_f \end{bmatrix} = \begin{bmatrix} L_{11} & 0 & 0 \\ L_{21} & L_{22} & 0 \\ L_{31} & L_{32} & L_{33} \end{bmatrix} \begin{bmatrix} Q_1 \\ Q_2 \\ Q_3 \end{bmatrix} \tag{7}$$

In eq. (7), $L_{ij}$ are lower triangular matrices and $Q_i$ are rectangular semi-orthogonal matrices with dimension $N$ along rows. The past data matrix is defined as $Z_p = [U_p^T \; Y_p^T]^T$. The LQ decomposition step gives an efficient decomposition for identification of terms in equation (6).

To further identify the system, N4SID algorithms uses fundamental assumptions. These assumptions formalize sufficiently pertinent experiments to be able to identify state-space subspaces.

*Hypotheses.*

$$\text{rank}\,(X_p) = n \tag{H1}$$

$$\text{rank}\,(U_p) = \text{rank}\,(U_f) = hn_i \quad \text{where } hn_i \geq n \tag{H2}$$

$$\text{span}'(X_p) \cap \text{span}'(U_p) = \text{span}'(X_f) \cap \text{span}'(U_f) = \{0\} \tag{H3}$$

In the above, $\text{span}'(M)$ denotes the vector space obtained from linear combinations of rows of $M$. Assumption (H1) follows from having all the $n$ states of system excited in the past data batch. The excitation is assumed to be persistent exciting of order superior to $n$ meaning the excitation matrices $U_p$ and $U_f$ are full row rank with number of rows exceeding $n$, leading to assumption (H2). For further details over persistent exciting condition see references [3]. The last assumption (H3) means that excitations are assumed independent of the state dynamics. In linear algebra, $\text{span}'(X_f)$ and $\text{span}'(U_f)$ are said to be in direct sum. The direct sum between spaces is defined by having uniqueness of any decomposition of vectors belonging to these spaces. This is equivalent to have their intersection reduced to the null vector. The hypothesis (H3) can be verified by taking a row vector as sum of $\text{span}'(X_f)$ and $\text{span}'(U_f)$ element, it can be shown that the decomposition is unique using the scalar product induced by $\mathbb{E}[a^T b]$.

Data compression through LQ decomposition and the above assumptions lead to a decomposition of $Y_f$ over matrices $U_f$, $Z_p$ and $Q_3$. Indeed, assumption (H2) gives that $L_{11}$ is invertible leading to equation (8), and matrix $Q_2$ can be deduced using the generalized inverse formula for $R_{22}$ leading to equation (9).

$$Q_1 = L_{11}^{-1} U_f \tag{8}$$

$$\begin{aligned} L_{32}Q_2 &= L_{32}\left[L_{22}^{+}\left(Z_p - L_{21}Q_1\right) + \left(I - L_{22}^{+}L_{22}\right)\Xi\right] \\ &= L_{32}L_{22}^{+}\left(Z_p - L_{21}L_{11}^{-1}U_f\right) \end{aligned} \tag{9}$$

The arbitrary matrix $\Xi$ has been introduced to set up the multiple solutions obtained by general inverse. It can be shown that $\ker(L_{22}) \subset \ker(L_{32})$ (see [4] or appendix A) which makes the term $L_{32}\left(I - L_{22}^{+}L_{22}\right)\Xi$ vanish as $L_{32}$ is applied on $I - L_{22}^{+}L_{22}$, the projection over $\ker(L_{22})$. Then, a decomposition of $Y_f$ follows from equations (7-9):

$$\begin{aligned} Y_f &= L_{32}L_{22}^{+}Z_p + \left(L_{31} - L_{32}L_{22}^{+}L_{21}\right)L_{11}^{-1}U_f + L_{33}Q_3 \\ &\text{with} \quad \tfrac{1}{N}Z_pQ_3^T = 0 \quad \text{and} \quad \tfrac{1}{N}U_fQ_3^T = 0. \end{aligned} \tag{10}$$

Comparing orthogonality properties below equation (10) and (6), the purely stochastic part of $Y_f$ can be identified $V_f' = L_{33}Q_3$. Furthermore, it is possible to filter out all the terms with right factor $U_f$ using the orthogonal projection matrix $\Pi_{U_f}^{\perp} = I - U_f^{+}U_f$. Then, using $\zeta$ to denote $\mathcal{O}_h X_f$, the identity relation given by the two decompositions of $Y_f$ (equations 6 and 10) yields:

$$\zeta\Pi_{U_f}^{\perp} = \mathcal{O}_h X_f \Pi_{U_f}^{\perp} \overset{(a)}{=} L_{32}L_{22}^{+}Z_p\Pi_{U_f}^{\perp} \overset{(b)}{=} L_{32}L_{22}^{+}L_{22} = L_{32} \tag{11}$$

*"Projected" optimal prediction* (`N4SID.MOESP`).

In the above series of equality, the second equality marked (a) is deduced from the identity relation over $Y_f$ (eq. 10) along with the projection property $U_f\Pi_{U_f}^{\perp} = 0$. The third equality marked (b) is obtained by using the LQ decomposition $Z_p = L_{21}Q_1 + L_{22}Q_2$ with $Q_1 = L_{11}^{-1}U_f$ (eq. 8) and $Q_2U_f^T = 0$. Note that it is possible to identify directly $\zeta$ without the projection $\Pi_{U_f}^{\perp}$. Appendix B gives further details concerning this more general result.

After predicting the optimal states' trajectory N4SID framework proposes to estimate a realization of the product $\mathcal{O}_h X_f$ using the compact singular value decomposition of the right-hand side of equation (11):

$$L_{32} = U\Sigma V^T \approx U_n \Sigma_n V_n^T \tag{12}$$
$$\textit{Complexity reduction} \ (\texttt{N4SID.MOESP}).$$

where $U \in \mathbb{R}^{hn_o \times r}$ and $V \in \mathbb{R}^{N \times r}$ are semi-orthogonal matrices, *i.e.* $U^T U = V^T V = I_r$. The matrix of singular values $\Sigma \in \mathbb{R}^{r \times r}$ is diagonal with positive coefficients. As there is noise over the system dynamics the rank verifies $r = \min(hn_o, N)$, usually $r = hn_o$. To filter out states coming from the noise process a truncation step is performed consisting in reducing $r$ to $n$, the assumed number of states of the system. Some techniques to determine this order $n$ are presented in section 2. The matrices $U_n \in \mathbb{R}^{hn_o \times n}$, $\Sigma_n \in \mathbb{R}^{n \times n}$ and $V_n \in \mathbb{R}^{N \times n}$ in equation (12) denote the truncated singular value decomposition. Any realization of $U_n \Sigma_n V_n^T$ in a two-factor product can be used as estimate of $\mathcal{O}_h$ and $X_f$. Equation (13) combines the optimal projection and the complexity reduction to propose a balanced realization leading to the following estimates of the observability and states matrices.

$$\mathcal{O}_h X_f \Pi_{U_f}^{\perp} \approx \left(U_n \Sigma_n^{1/2}\right)\left(\Sigma_n^{1/2} V_n^T\right) \tag{13}$$
$$\widehat{\mathcal{O}}_h = U_n \Sigma_n^{1/2} \tag{13a}$$
$$\widehat{X_f \Pi_{U_f}^{\perp}} = \Sigma_n^{1/2} V_n^T \tag{13b}$$

From equations (13a,b) two techniques to estimate the state-space matrices are possible. The first technique estimates $A, C$ from the extended observability matrix estimate (eq. 13a). Indeed, the structure of equation (3) gives the following estimates.

$$\widehat{C} = \widehat{\mathcal{O}}_{h(1:n_o,\ :)} \tag{14a}$$
$$\widehat{A} = \left(\widehat{\mathcal{O}}_h^{(0)}\right)^{+} \widehat{\mathcal{O}}_h^{(1)} \tag{14b}$$
$$\text{with} \quad \widehat{\mathcal{O}}_h^{(0)} = \widehat{\mathcal{O}}_{h(1:\text{end}-n_o,\ :)} \quad \widehat{\mathcal{O}}_h^{(1)} = \widehat{\mathcal{O}}_{h(n_o:\text{end},\ :)}$$

In the above, "end" denotes the last index and the symbol ":" alone denotes all the index along the dimension. For the estimation of state-space matrices $B$, $D$ as well as the estimation of matrix $\Psi_h$ see reference [4, p. 158]. The second technique estimates the states $X_f$ from the right part of the singular value decomposition of the complexity reduction step, more details over this technique are given in references (cf. [10, 13]). The computation process involving left part of the singular value decomposition is usually lighter than the one using the right part, as $U_n$ has size $hn_o \times n$ while $V_n^T$ has size $n \times N$.

### *1.3. Maximum correlation criterion*

Canonical variate analysis extends the criterion used for optimal estimation by generalizing the least square principle. This technique was proposed by W. Larimore in 1990 [13] in the continuity of the work of H. Akaike investigating canonical correlation analysis for system identification [14–16]. It tackles the identification problem by building canonical variables obtained from an extended prediction criterion. This criterion can be interpreted as the minimum error variance principle transformed under an arbitrary quadratic weighting matrix $\Lambda^{+}$, taken as the pseudoinverse of a positive semidefinite symmetric matrix $\Lambda$. In addition to this change of prediction criterion, a constraint is added to force the rank of the linear regression to be equal to the order of the system.

$$p_t = \text{col}(y_{t-1},\ y_{t-2},\ ...,\ u_{t-1},\ u_{t-1},\ u_{t-2},\ ...)$$
$$f_t = \text{col}(y_t,\ y_{t+1},\ y_{t+2},\ ...)$$
$$\min_{\substack{\hat{f}_t = J_n p_t \\ \text{rank}(J_n) = n}} \mathbb{E}\left[\|\hat{f}_t - f_t\|_{\Lambda^{+}}^2\right] \tag{15}$$

In eq. (15), "col" is the operator for stacking column vectors and $J_n$ is a linear transformation to build the estimate of future observations $\hat{f}_t$ from past data $p_t$. Equation (15) is to be interpreted as a constrained optimization problem for $J_n$. The notation $\|.\|_{\Lambda^+}$ denotes the norm induced by $\Lambda^+$. For column vector $m$, this norm is defined as $\|m\|^2_{\Lambda^+} = m^T \Lambda^+ m$. The resolution of problem (15) can be drawn from a generalization of the singular value decomposition which uses weighting matrices (cf. [13]). Choosing the matrix which defines the quadratic weighting as $\Lambda = \Sigma_{ff} = f_t f_t^T$ leads to define optimal prediction from a principle of maximum coefficient of correlation.

$$\operatorname{corr}[a, b] = \frac{\operatorname{cov}[a, b]}{(\operatorname{var}[a] \operatorname{var}[b])^{1/2}}$$

The above equation defines the coefficient of correlation between two random variables $a$ and $b$.

The unified framework N4SID has been shown to include the above-mentioned identification method making its implementation a variant of the method describes in previous section 1.2 (cf. [12]). To this end, the above identification procedure has been regrouped into two steps an *optimal prediction* followed by a *complexity reduction*. This implementation is further called N4SID Canonical Variate Analysis (`N4SID.CVA`). The *optimal prediction* principle consists in estimating the best combinations of the past observations and future excitations to predict accurately the future using all available information. The optimality of the prediction step is evaluated by means of the Frobenius norm. In consequence, `N4SID.MOESP` and `N4SID.CVA` use the same procedure for "optimal prediction", *i.e.* perform the LQ decomposition and use the fundamental hypotheses to obtain the contribution of states in the measurements.

*"Projected" optimal prediction* (`N4SID.CVA`)

$$\zeta \Pi_{U_f}^{\perp} = L_{32} \tag{16}$$

Where the contribution of states $\zeta$ has been defined earlier, $\zeta \coloneqq \mathcal{O}_h X_f$. The *complexity reduction* principle moderates the prediction capacity of the model by imposing the order of the system, *i.e.* the maximum amount of past information to use for prediction. Comparing to the explanation of `N4SID.MOESP` (cf. 1.2), the complexity reduction step of the full N4SID framework is more elaborated. The singular value decomposition of states contribution $\zeta$ is performed with weighting matrices $W_1$ and $W_2$. The weighting matrix $W_2$ is taken as $\Pi_{U_f}^{\perp}$ in order to be compliant with the projected optimal prediction step. As mentioned in the beginning of this section, choosing the weighting matrix $\Lambda$ (eq. 15) to tackle maximum correlation coefficient will lead to put the second moment of future observations as weighting matrix. The reference article presenting the unified framework of N4SID (cf. [12]) has discussed the exact weighting matrix $W_1$ needed to have equivalence with the CVA technique.

*Complexity reduction* (`N4SID.CVA`)

$$\begin{aligned} W_1 \zeta W_2 &= U \Sigma V^T \approx U_n \Sigma_n V_n^T \\ \text{with, } W_1 &= (Y_f \Pi_{U_f}^{\perp} Y_f^T)^{-1/2} \\ W_2 &= \Pi_{U_f}^{\perp} \end{aligned}$$

The determination of the extended observability matrix followed by the estimation of state-space matrices $A, C$ is identical to section 1.2.

The N4SID framework makes possible to switch from minimum variance criterion to maximum correlation criterion by changing the weighting matrix $W_1$. It is interesting to note that the principle of maximum of correlation coefficient can be extended by the concept of maximum of mutual information between two random variables. The mutual information analyzes the distance between two probability laws through the following quantity.

$$\mathrm{I}_{(L,M)} = \int_{l \in L} \int_{m \in M} \mathrm{p}_{L,M}(l,m) \log \left( \frac{\mathrm{p}_{L,M}(l,m)}{\mathrm{p}_L(l) \mathrm{p}_M(m)} \right) \mathrm{d}l \mathrm{d}m$$

The mutual information measures the divergence between probability laws given by $\mathrm{p}_{(L,M)}$ and $\mathrm{p}_{(L)}\mathrm{p}_{(M)}$ the same way entropy measures the amount of information of a random variable [17]. For normally distributed

variables $L$ and $M$, the mutual information becomes $\mathrm{I}_{(L,M)} = -(1-(\mathrm{corr}[L,M])^2)/2$. Then, maximizing the mutual information between L and M is equivalent to maximizing their coefficient of correlation.

## 2. Order determination techniques

During the presentation of identification techniques in previous section, the order of the state-space representation has been processed as a known parameter. However, the number of modes participating in the identification experiment is unknown in modal tests. Furthermore, taking a wrong system order can lead to modeling errors in the identification results as the identification algorithm will fit purely noise processes using system dynamics. To this end, strategies to determine model order have been proposed to give indications over the optimal order for identification. This section briefly describes two strategies building indicators for the determination of the optimal order.

The first indicator is a variant of the original Akaike's information criterion (AIC) [18], the normalized AIC. This indicator proposes to scale the AIC criterion by the number of temporal samples used for computing empirically the statistical expectation.

$$nAIC = \log\left(\mathcal{V}\right) + \frac{2n_p}{N} \tag{17}$$

In the above, $n_p$ is the number of unknown parameters in $A, B, C$ matrices, $n_p = n^2 + (n_o + n_i)n$, and $\mathcal{V}$ is the least square cost function between predicted and observed dynamics. The optimal order is taken as the order minimizing the $nAIC$ indicator. This minimization can be interpreted as minimizing an estimation cost function with a penalty over the number of parameters in the system.

The second indicator proposes to observe the evolution of the fitting error with respect to the order of the state-space model. The fitting error is measured as the relative mean square error between the estimated and the measured frequency response to a stepped sine excitation. This frequency response is obtained by computing the forced response over a finite duration at the end of each frequency step, for more details over the measurement of the frequency response function we refer to a previous study [2].

$$rRMSE_\nu = \left( \frac{\sum_{i=1}^{n_{\text{steps}}} |\widehat{FRF}_{(\omega_i)} - FRF_{(\omega_i)}|^2}{\sum_{i=1}^{n_{\text{steps}}} |FRF_{(\omega_i)}|^2} \right)^{1/2} \tag{18}$$

In the above, $FRF_{(\omega_i)}$ denotes the frequency response function at step with pulsation $\omega_i$, and $\widehat{\cdot}$ denotes the estimated corresponding quantity. This strategy selects the optimal order as the order after which the gain in fitting error is no longer significant.

## 3. Uncertainties propagation

This section proposes a technique to use the estimation of covariance matrices of the stochastic processes in the modal analysis. First, the innovation formulation of state-space models is presented. Then, the concept of pseudospectrum of a matrix is presented in a general way. The third subsection details the use of uncertainties estimate and pseudospectrum for the evaluation of modal uncertainties.

### *3.1. Uncertainties of state-space estimation*

The information of the uncertainties of the state-space estimation are carried out by the covariance matrices, *i.e.* $Q, R, S$ for state-space models in process form (eq. 2) and by the Kalman gain and the innovation vector for "Innovation" form. The "Innovation" form of a state-space representation describes the dynamics of the system with optimal states in the sense of minimum variance of the prediction error. These states are called Kalman states from the work of R. E. Kalman [19, 20]. The innovation form is presented in

the equation below with $\hat{x}_{(t|t-1)}$ the Kalman states estimate at time step $t$ using information at time step $t-1$.

$$\begin{aligned} \hat{x}_{(t+1|t)} &= A\hat{x}_{(t|t-1)} + Bu_t + Ke_t \\ \hat{y}_t &= C\hat{x}_{(t|t-1)} + Du_t \\ e_t &= y_t - \hat{y}_t \end{aligned} \tag{19}$$

Where the innovation process $e_t$ characterizes the error between the predicted observation $\hat{y}_t$ and the actual observations $y_t$. The Kalman gain $K$ models the effect of noise in the estimated states transition equation. The optimality condition over the Kalman states can be used to translate state-space representation in process form into innovation form. Indeed, this condition gives a relation for $K_t$ depending on state matrices and covariance matrices of state-space model in equation (2) as well as $P_t$ the error covariance matrix of the "true" states vector $x_t$.

$$\begin{aligned} K_t &= \left(AP_tC + S\right)\left(CP_tC^T + R\right)^{-1} \\ &\text{with, } P_t = \mathbb{E}\left[(\hat{x}_t - x_t)(\hat{x}_t - x_t)^T\right] \end{aligned} \tag{20}$$

The estimate of the covariance matrix $P_t$ is obtained by solving a discrete algebraic Riccati equation drawn from stationary assumption $P_{t+1} = P_t$ further denoted $P$.

$$P = APA^T - \left(APC^T + S\right)\left(CPC^T + R\right)^{-1}\left(APC^T + S\right)^T + Q \tag{21}$$

Equation (21) can be solved numerically for the unknown matrix $P$ using state-space matrices estimate $\widehat{A}, \widehat{C}$ and covariance matrices estimates $\widehat{Q}, \widehat{R}, \widehat{S}$. To estimate these matrices for `N4SID.MOESP` and `N4SID.CVA` one possibility consists in estimating the states $\widehat{X}_f = \widehat{X}_{t+h|h,N}$ from the optimal prediction by using the pseudoinverse of the estimated matrix $\hat{\mathcal{O}}_h$.

$$\widehat{X}_f = \left(\hat{\mathcal{O}}_h\right)^+ \zeta$$

Having the estimates of state-space matrices $\widehat{A}, \widehat{B}, \widehat{C}, \widehat{D}$ and states coordinates $\widehat{X}_f$, one can deduce the residues, $\rho_w$ and $\rho_v$, of the one step state-space relation.

$$\begin{bmatrix} \widehat{X}_1 \\ Y_0 \end{bmatrix} = \begin{bmatrix} \widehat{A} & \widehat{B} \\ \widehat{C} & \widehat{D} \end{bmatrix} \begin{bmatrix} \widehat{X}_0 \\ U_0 \end{bmatrix} + \begin{bmatrix} \rho_w \\ \rho_v \end{bmatrix} \quad \text{with} \begin{cases} M_0 = M_{t+h|1,N-1} \\ \quad \text{for } M = \widehat{Y}, \widehat{U} \text{ or } \widehat{X} \\ \widehat{X}_1 = \widehat{X}_{t+h+1|1,N-1} \end{cases}$$

The residues can be used to estimate the covariance matrices.

$$\begin{bmatrix} \widehat{Q} & \widehat{S} \\ \widehat{S}^T & \widehat{R} \end{bmatrix} = \frac{1}{N} \begin{bmatrix} \rho_w \rho_w^T & \rho_w \rho_v^T \\ \rho_v \rho_w^T & \rho_v \rho_v^T \end{bmatrix}$$

Having an estimation of the covariance matrices, the Kalman gain can be estimated in turn (cf. 20, 21). The Kalman gain $K$ and the innovation process $e_t$ will be used in the following to propagate the uncertainties of state-space estimation to modal parameter estimation.

### *3.2. Pseudospectrum as uncertainty propagator*

The discrete time state-space representation in equation (19) can be converted into continuous time using a zero-order hold interpolation and by integrating the continuous state-space model between each time step. The continuous state-space matrices $A_c, B_c, K_c$ are then given as solutions of the following matrix equation system where the sampling period is denoted $T_e$.

$$\begin{aligned} A &= \exp\left(A_c T_e\right) \\ B &= A_c^{-1}\left(\exp\left(A_c T_e\right) - I\right) B_c \\ K &= A_c^{-1}\left(\exp\left(A_c T_e\right) - I\right) K_c \end{aligned}$$

The estimation of the state-space matrices $A_c$ and $B_c$ can be transformed to a modal form using the solution of the eigenproblem of the continuous state transition matrix. This solution is further denoted $\Lambda$ for the diagonal matrix of eigenvalues and $\Phi$ for eigenvectors matrix.

$$\begin{aligned} \dot{q}_{(t)} &= \Lambda q_{(t)} + B'_c u_{(t)} + K'_c e_{(t)} \\ y_{(t)} &= C'_c q_{(t)} + D u_{(t)} + e_{(t)} \\ \text{with,} \quad \Lambda &= \Phi^{-1} A_c \Phi \quad B'_c = \Phi^{-1} B_c \\ C'_c &= C_c \Phi \qquad\quad K'_c = \Phi^{-1} K_c \end{aligned}$$

In the above equations, the modal coordinates $q_{(t)} = \Phi^{-1} x_{(t)}$ have been introduced.

The $\varepsilon$-pseudospectrum can provide the modal analysis with evaluation of the uncertainties in the state transition equation. This mathematical concept consists in evaluating the locus of the complex values which "almost solve" the eigenproblem. Three equivalent definitions can be used to define the $\varepsilon$-pseudospectrum of a matrix $A$, further denoted $\sigma_\varepsilon(A)$.

*i*. The set of solution of the perturbed eigenproblem.

$$\sigma_\varepsilon(A) = \{z \in \mathbb{C} \mid \exists E \in \mathbb{R}^{n\times n}, \|E\| < \varepsilon \text{ and } z \in \lambda(A+E)\} \tag{$i$}$$

*ii*. The set of values reaching a sufficiently low residual norm for the eigenproblem.

$$\sigma_\varepsilon(A) = \{z \in \mathbb{C} \mid \exists u \in \mathbb{C}^n, \|u\| = 1 \text{ and } \|(A - zI)u\| < \varepsilon\} \tag{$ii$}$$

*iii*. The set of values making the resolvent reach sufficiently large norm.

$$\sigma_\varepsilon(A) = \{z \in \mathbb{C} \mid \|(A - zI)^{-1}\| > 1/\varepsilon\} \tag{$iii$}$$

For more details concerning $\varepsilon$-pseudospectrum concept we refer to references [21] and [22]. Taking into account uncertainties in the modal analysis leads to consider the perturbed homogeneous equation of states transition.

$$\begin{aligned} \sigma\varphi &= A_c\varphi + K_c e \\ (A_c - \sigma I)\varphi &= -K_c e \end{aligned} \tag{22}$$

Equation (22) is obtained by keeping only the stochastic process $K_c e$ in the right-hand side. As the stochastic process $-K_c e$ verifies $\mathbb{E}[K_c e] = 0$ and is normally distributed, it is possible to use $\mathrm{var}[K_c e]$ to compute confidence intervals around zero for equation (22). Evaluating the norm of the above equation one can recognize the definition (*ii*) of $\varepsilon$-pseudospectrum of $A_c$.

$$\begin{aligned} &\|(A_c - \sigma I)\varphi\| < \varepsilon \\ &\text{with, } \varepsilon = \alpha \left(\|\mathrm{var}[K_c e]\|_2\right)^{1/2} \end{aligned} \tag{23}$$

In inequality (23), the bound $\varepsilon$ has been parametrized using the maximum standard deviation of the multivariate process $-K_c e$, considering all the possible directions, and the parameter $\alpha$. In this article, we have chosen to compute $\varepsilon$-pseudospectra with $\alpha = 3$. This choice corresponds to a 99.7% confidence interval for one dimension perturbation processes.

### *3.3. Evaluation of modal uncertainties*

The procedure to evaluate modal uncertainties in this study uses $\varepsilon$-pseudospectrum computation. This computation makes use of the $\varepsilon$-pseudospectrum defined using resolvent sufficiently large condition (cf. *iii*). To this end, the Euclidian norm of the resolvent is computed over polar grids of the complex plane centered

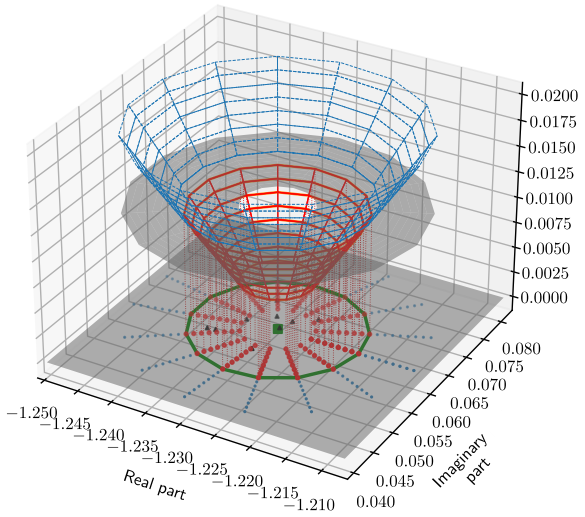


*Figure 1: Illustration of functional $z \mapsto s_{min}[A_c - zI]$ around one mode for $\varepsilon$-pseudospectrum computation. Eigenvalue ■ ; initialization ▲ ; $\varepsilon$-pseudospectrum inner ● , outer • , border — ; functional inner values — and outer values --- .*

around each eigenvalue. Choosing the Euclidian norm makes the computation of $\varepsilon$-pseudospectrum equivalent to computing the minimal singular value of the inverse of the resolvent which is $A_c - zI$ for $z \in \mathbb{C}$.

$$s_{min}[A_c - zI] \tag{24}$$

Where $s_{min}$ denotes the minimal singular value. This pseudospectrum computation technique has been tested using `svd` function of `numpy` [23].

Another strategy computes the required functional more efficiently by using the Schur decomposition of the matrix $A_c$ as well as inverse Lanczos iterations. The use of the inverse Lanczos iterations is inspired from observation that this computation is equivalent to finding the minimum positive eigenvalue of a larger hermitian matrix:

$$\min \ \text{eig}_+ \begin{bmatrix} 0 & A_c - zI \\ A_c^* - z^* I & 0 \end{bmatrix} \tag{25}$$

where $\text{eig}_+$ denotes the positive eigenvalues. Then, the computation can benefit from efficient iterative methods to compute the largest eigenvalue of a hermitian matrix, like Lanczos iterations. This pseudospectrum computation technique, known as "inverse Lanczos" strategy, has been tested using `eigsh` of `scipy.sparse` applied on the sparse linear operator associated with the inverse of the matrix in equation (25). For more details over the iterative method used to compute the eigenvalues we refer to Implicitly Restarted Arnoldi Method [24]. Although the algorithm based on the inverse Lanczos procedure have less complexity, the computational costs of the two implementations to compute the $\varepsilon$-pseudospectrum of an estimated matrix $A_c$ have shown to be equivalent. It is important to stress that this comparison holds for the estimated matrices which have size $n \times n$ which is relatively small, especially compared to matrices coming from finite element modeling.

The technique to compute $\varepsilon$-pseudospectra for the following of this article uses the "SVD strategy" (24). The grid selection procedure solves few perturbed eigenproblems defined in equation (*i*). Then, a polar grid around each eigenvalue is selected which includes the further perturbed eigenvalue and which have a radial and angular pace sufficiently low to describe accurately the border of the pseudospectrum. Figure 1 illustrates this pseudospectrum computation. The computed functional is plotted with a meshed surface over the selected grid. The plane $z = \varepsilon$ splits the plotted surface into an inner locus, namely the pseudospectrum,

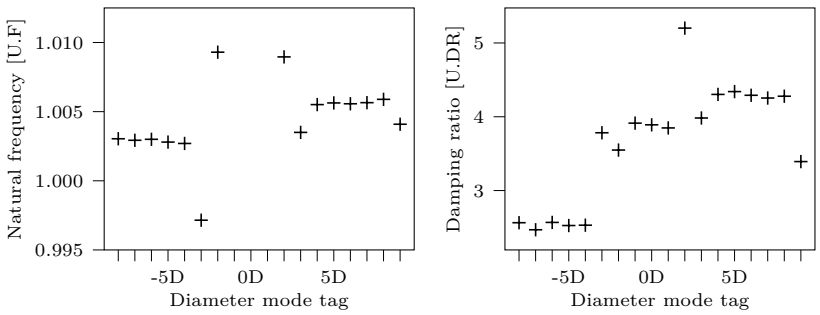


*Figure 2: Reference eigenvalues of the modal model.*

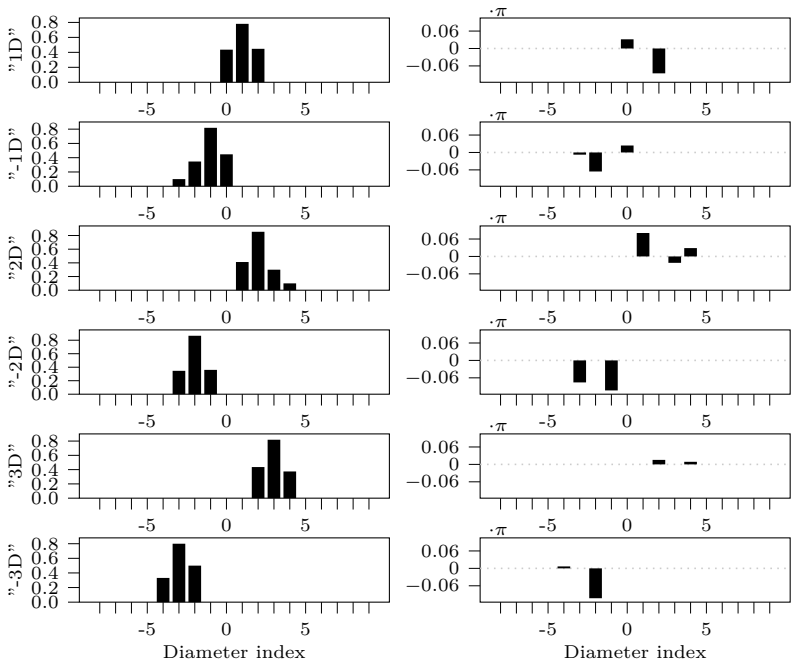


*Figure 3: Discrete spatial Fourier transform of mode shapes for modes tagged* $\pm 1D, \pm 2D, \pm 3D$*. Left: amplitude, right: phase* [rd].

and an outer locus. The pseudospectrum border is plotted onto the complex plane. This border has a circular shape for sufficiently small covariance matrices estimate as it is illustrated in figure 1 and has been observed in results of section 4.2.

Finally, the inner locus of the $\varepsilon$-pseudospectrum gives all the complex values which are compliant with a certain confidence interval for each eigenvalue. To process these eigenvalues uncertainties into natural frequencies and damping ratios uncertainties, this article proposes to take the maximum and minimum of the natural frequencies and damping ratios of this set of complex values. This process leads to error bars around the modal parameters has shown in the next section.

## 4. Comparison of estimation results

A versatile model to evaluate the presented identification methods is presented in a first subsection. Second subsection gives comparison results obtained with this model.

*4.1. Simulated test case*

A modal model of a bladed disk have been created to generate representative simulated signals making possible to evaluate the performances of estimation methods in conditions similar to experiments. This modal model is defined using previous experimental studies performing modal analysis of a full-scale aeronautic fan with 18 sectors [2]. Figure 2 shows the natural frequencies and damping ratios of modes included in the model with respect to their diameter mode tag. The modal parameters for tagged modes $\pm 1D, \pm 2D, \pm 3D, \pm 4D$ have been chosen from modal tests, while the others parameters have been chosen arbitrarily as follows. The eigenvalues of modes tagged $5D, 6D, ..., 8D$ have been chosen with natural frequency and damping ratios close to the mode $4D$, the eigenvalues associated with opposite tags have been chosen close to mode $-4D$, and the eigenvalue of mode $9D$ has been chosen close to the average of natural frequency and damping ratio of modes $\pm 4D$. All the mode shapes have been taken as the mode shapes of the associated conservative system with cyclic symmetry locally perturbed by side components in spatial Fourier space. The perturbation is chosen normally distributed with a standard deviation close to 0.5. This choice leads to modes shapes composed of few traveling waves all close to the main diameter component, see figure 3. The phase of the traveling wave components perturbing the conservative cyclic symmetric mode shapes are drawn from a uniform distribution on $[-0.1\pi, 0.1\pi]$ with a reference of phase given by the main component. To evaluate the identification methods in similar conditions comparing to previous experimental modal analysis, the modal model is excited through a purely traveling wave with stepped in frequency. The simulations are performed by numerical integration of the continuous real modal form.

$$\begin{aligned} \dot{s}_{(t)} &= \Lambda^{\mathbb{R}} s_{(t)} + {B'_c}^{\mathbb{R}} u_{(t)} + w_{(t)} \\ y_{(t)} &= {C'_c}^{\mathbb{R}} s_{(t)} + v_{(t)} \end{aligned}$$

$$\text{with,} \quad \Lambda^{\mathbb{R}} = P^H \Lambda P \quad {B'_c}^{\mathbb{R}} = P^H B'_c \qquad P = \operatorname{diag}\left(P^{(1)}, \ ..., P^{(1)}\right)$$

$$ {C'_c}^{\mathbb{R}} = C'_c P \qquad s = P^H q \qquad P^{(1)} = \frac{1}{2}\begin{bmatrix} 1-j & 1+j \\ 1+j & 1-j \end{bmatrix}$$

The perturbation processes $w$ and $v$ have been taken as white noise normally distributed with diagonal covariance matrices and overall noise over signal ratio at $NSR_w = 0.03$ and $NSR_v = 0.05$. The integration is performed with an explicit Runge-Kutta 45 method with zero initial conditions. The time step parameter has been checked by means of analytical solution. Excitation and response signals are shown for a forward traveling wave with three nodal diameters on figure 4. Normalized units $U.T$ and $U.F = 1/U.T$ are used in this article. The frequency steps of the excitation signal can be observed on the envelope of the response signals (fig. 4a). The temporal signal exhibits two particular events, at $\sim 0.35$ $U.T$ an aliasing artifact where the sampling frequency is a multiple of the excitation frequency step, and before 0.05 $U.T$ where the transient effect induced by taking initial conditions at zero generates a small artifact in the response signal. The Gaussian windowed Fourier transform used for time-frequency representation (fig. 4b) is well presented in reference articles [25, 26]. Using this representation the frequency steps depict vertical fringes around the average sweeping rate.

*4.2. Estimations of modal parameters*

The investigated subspace identification methods `N4SID.MOESP` and `N4SID.CVA` have been evaluated over the simulated signals. The identification experiments are performed using the complete time signal of all the generated responses and the excitation signal of one reference sector. The identification methods are applied with a chosen order $n = 6$. This order determination is expected as only three modes have traveling wave component $d = 3$ different from zero. Figure 5 illustrates the results of the two order indicators described in section 2 for this test case. On this simulated data the two strategies would find the appropriate order for the identification method. The first strategy would lead to $n = 6$, as it minimizes the $nAIC$, and the second strategy also, as no significant decrease of $rRMSE_\nu$ is observed after $n = 6$.

The default identification procedure of the N4SID implementation proposed by Matlab in `n4sid.m` proposes to choose a horizon $h_f = 9$ for the future data matrices and a horizon $h_p = 23$ for the past data matrices. In section 1.2, the past and future horizons have been taken identical to simplify explanations. However, the

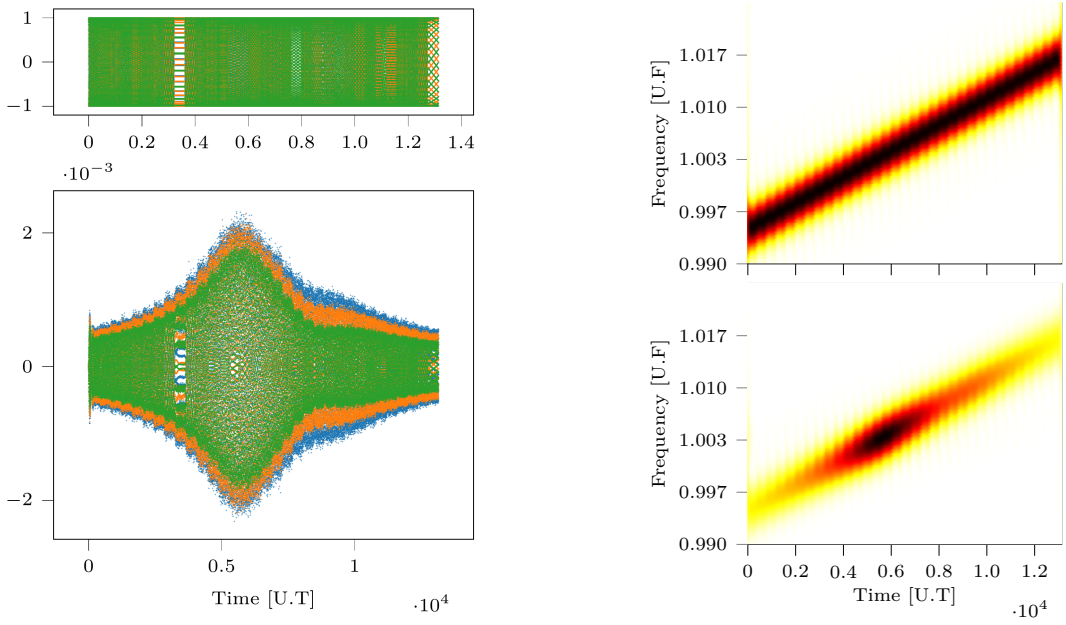


*(a) Time space.*
*Up: excitation, down: response.*

*(b) Time-frequency space.*
*Up: excitation, down: response.*

*Figure 4: Excitation and response signals for a 3D stepped sine excitation : time signals for three consecutive blades (a) and Gaussian windowed Fourier transforms of one blade (b).*

same identification procedures can be applied with different past and future horizons. The computational costs for one estimation was inferior to 15 minutes on a supercomputer using 45 processors and 30 GB of RAM. Such computational costs are required because the complete signals have large dimensions in order to be able to investigate the stationary state of the system at each frequency step and keep variance information of signals.

The estimated modes are sorted using a Modal Assurance Criterion (MAC) to compare modal estimation with the reference parameters. Figures 6 and 7 show estimation results over signals generated with excitation as a forward traveling wave with three nodal diameters. Figure 6 compares the three estimated mode shapes with the only three reference mode shapes which can respond to the used excitation pattern. The amplitude and phase of the discrete spatial Fourier transform of the estimated mode shapes closely match the reference mode shapes. Figure 7a shows eigenvalues estimation over 29 simulations. All simulations use the same model, excitation and noise over signal ratio parameters. The only difference comes from different noise realizations of perturbation processes $w$ and $v$. The evaluation of modal uncertainties described in section 3.3 has been performed for each of the estimation results. On this test case, both methods give equivalent estimates for natural frequency and damping ratio. Natural frequency estimates have less deviation from the reference values along the different repetitions of the identification experiments compared with damping ratio estimates. The estimates of natural frequency and damping ratio of mode tagged "3D" are closer to the reference than modes tagged "2D" and "4D". This behavior can be explained by a higher participation of mode tagged "3D" in the system response, and so a better ratio between mode dynamics and noise level. For both methods the modal uncertainties over damping ratio estimates are higher than natural frequency, of the order of $\delta\xi/\xi \sim 5{\cdot}10^{-2}$ compared with $\delta\omega/\omega \sim 5{\cdot}10^{-4}$. Although `MOESP` and `CVA` weightings lead to eigenvalues estimates which are identical, the uncertainty propagation procedure leads to significant different confidence intervals. Estimates from `MOESP` weighting have smaller modal uncertainties compared with `CVA` weighting, see damping ratio estimates of figure 7b. The propagated confidence intervals for damping ratios of the targeted mode (tagged "3D") do not always contain the reference value for `MOESP` weighting whereas it

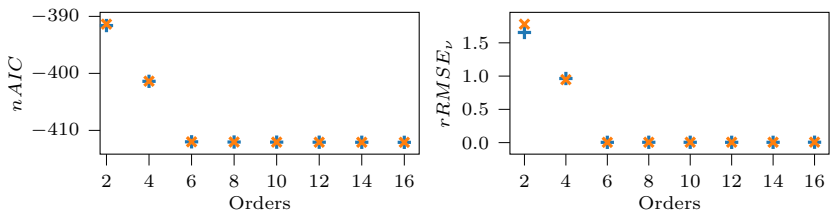


*Figure 5: Evolution of order indicators. MOESP + ; CVA × .*

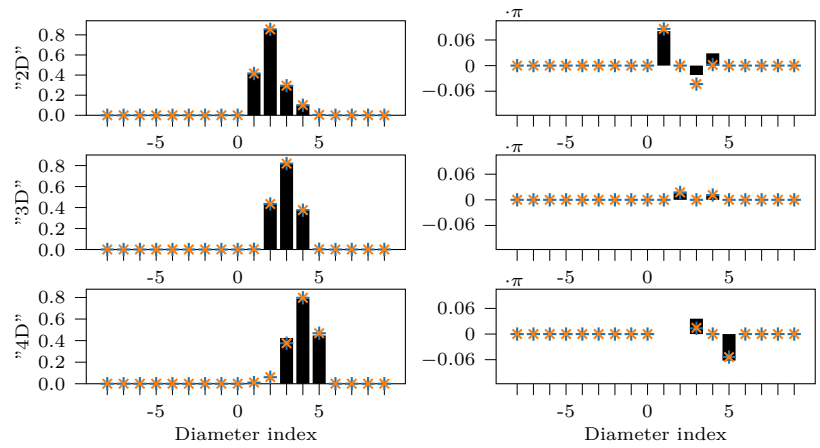


*Figure 6: Spatial Fourier transform of estimated mode shapes paired with the reference mode shapes according the MAC criterion. Left: amplitude, right: phase* [rd]. *MOESP + ; CVA + .*

is verified for `CVA` weighting (see diameter mode tag $3D^{(1)}, 3D^{(4)}, 3D^{(6)}$ and $3D^{(9)}$ on damping ratio figure 7b). Observing estimated modes 4D and 2D the uncertainty bars do not always include the reference. This can be explained by a more detrimental ratio between the dynamics of these modes and the level of noise as the excitation targets only diameter index $d = 3$. Simulations with lower overall noise level or more appropriate excitations have shown to bring better estimate for these two modes as well as the other modes of the system. In summary, `CVA` weighting seems to provide more accurate uncertainty estimates than `MOESP` weighting for simulated identification experiments of one targeted mode.

## Conclusion

In this article, two state-space subspace identification methods have been reviewed. The first one, `N4SID.MOESP`, relies on minimum of variance of prediction error criterion, while the second one, `N4SID.CVA`, relies on maximum of correlation coefficient criterion. Both techniques give estimates of state-space matrices with the covariance matrices of the perturbation processes. This article presents a technique to propagate covariance estimates to modal estimates by means of $\varepsilon$-pseudospectrum computation. The $\varepsilon$-pseudospectrum gives the complex values which are nearly eigenvalues of a matrix. The modal uncertainties have been evaluated by computing the $\varepsilon$-pseudospectrum of the state transition matrix choosing $\varepsilon$ based on the estimation of the state transition covariance matrix. A modal model of a bladed disk has been proposed to assess the modal estimation performances under realistic conditions as well as to test the proposed propagation process of state-space uncertainties to modal parameters. While the methods yield quite similar modal estimates, the confidence intervals deduced from uncertainties propagation for the `N4SID.CVA` technique better match the reference results compared with `N4SID.MOESP`. This study may indicate that the natural choice of minimizing the prediction error may not always be the best choice for identification method, especially when

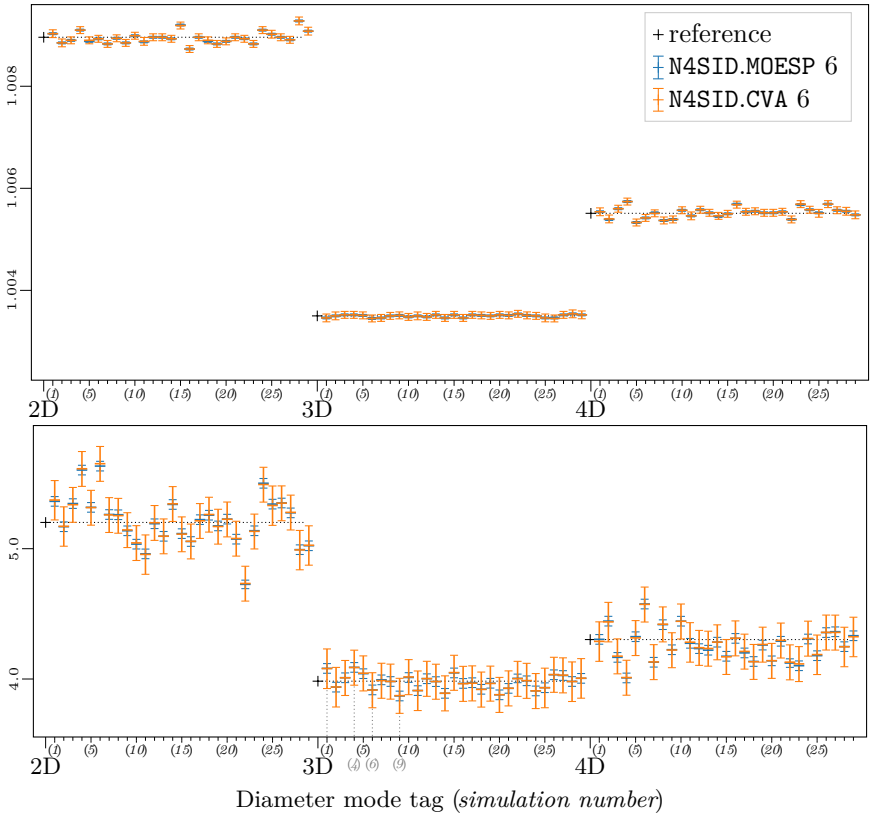


*(a) Estimations of natural frequency in U.F (up) and damping ratio in U.DR (down) for 29 simulations.*

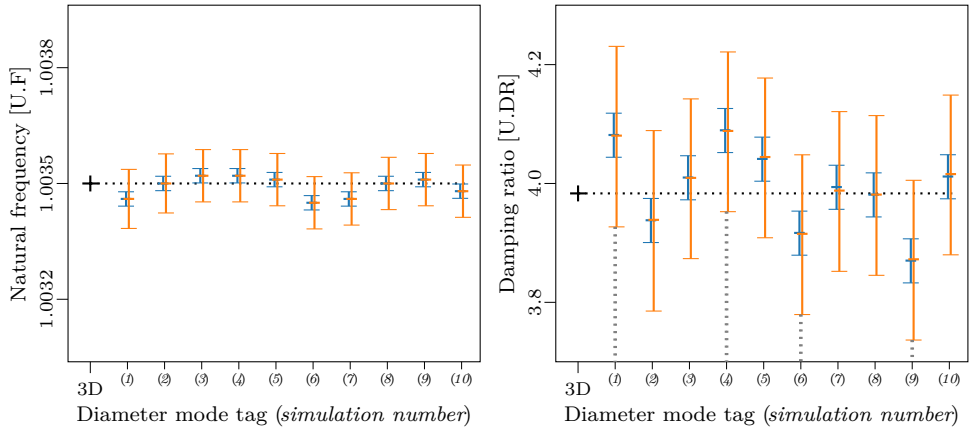


*(b) Focus on the most excited mode for the 10 first simulations. Mode tagged 3D is the most excited as the excitations have 3 nodal diameters.*

*Figure 7: Eigenvalues estimations over simulations using excitation pattern with 3 nodal diameters and different noise realizations. Figure (b) magnifies parts of figure (a). Estimation results are arbitrary shifted to the right using the simulation number.*

analyzing the uncertainties of estimation results. The simulated test case has shown that maximization of the coefficient of correlation may lead to better estimates of the modal uncertainties.

This study has focused on the comparison of modal estimation performances when the determination of the identification order and the identification itself are made easy by few modes responding to an appropriate excitation. It would be interesting to pursue the study in a context of more difficult identification and model order determination.

**Acknowledgment**

The authors are grateful to "Agence National de la Recherche" (France) for supporting PHARE#1 test rig through PIA EQUIPEX PHARE project (ANR-10-EQPX-0043), to Carnot Institute I@L and Safran Aircraft Engines for providing additional financial support as well as for giving permission to publish this work.

**Nomenclature**

| | |
|---|---|
| MOESP | Multi Output Error State space |
| CVA | Canonical Variate Analysis |
| $nAIC$ | normalized Akaike Information Criterion |
| $rRMSE_\nu$ | relative Root Mean Square Error in frequency |
| U.T, U.F | normalized unit of time and frequency |
| U.DR | normalized unit of damping ratio |
| $\mathrm{p}_A(a)$ | density probability of "variable $A$ takes value $a$" |
| $\mathbb{E}[a]$ | statistical expectation of random variable $a$ |
| $\mathrm{cov}[a,b]$ | covariance of $a$ and $b$: $\mathrm{cov}[a,b] = (a-\mathbb{E}[a])(b-\mathbb{E}[b])^T$ |
| $\mathrm{var}[a]$ | variance of random variable $a$: $\mathrm{var}[a] = \mathrm{cov}[a,a]$, |
| $L^2$ | square integrable function space |
| $\Gamma_{yy(\tau)}$ | autocorrelation of signal $y$: $\Gamma_{yy(\tau)} = \mathbb{E}\left[y_t y_{t+\tau}^T\right]$ |
| $j$ | imaginary unit: $j^2 = -1$ |
| $I$ | identity matrix |
| $M^H$ | hermitian conjugate of matrix $M$ |
| $M^+$ | pseudo-inverse of matrix $M$ |
| $\mathrm{span}'(M)$ | vector space spanned by rows of matrix $M$ |
| $\|.\|_\mathrm{F}$ | Frobenius norm |
| $\|.\|_{\Lambda^+}$ | norm induced by $\Lambda^+$ |
| $\delta_{ts}$ | delta Kronecker function |
| $n_o$ | number of observations |
| $n_i$ | number of excitations |
| $n$ | order of the system |

## References


[1] L. Carassale, R. Guida, M. Marrè-Brunenghi, Modal Identification of Bladed Disks by Time–Frequency Analysis of the Nonsynchronous Response, Journal of Engineering for Gas Turbines and Power 145 (2) (2022) 021020. doi:10.1115/1.4055684.

[2] C. Jorajuria, C. Gibert, F. Thouverez, C. Esteves, Experimental modal analysis of a full-scale rotating fan, in: Turbo Expo: Power for Land, Sea, and Air, Vol. 86076, American Society of Mechanical Engineers, American Society of Mechanical Engineers, 2022. doi:10.1115/gt2022-82540.

[3] L. Ljung, System Identification: Theory for the User, Prentice Hall PTR, Upper Saddle River, 1999.

[4] T. Katayama, Subspace Methods for System Identification, Communications and Control Engineering, Springer London, 2005. doi:10.1007/1-84628-158-x.

[5] M. Verhaegen, A novel non-iterative MIMO state space model identification technique, IFAC Proceedings Volumes 24 (3) (1991) 749–754. doi:10.1016/s1474-6670(17)52439-8.

[6] M. Verhaegen, P. Dewilde, Subspace model identification, part 1. The ouput-error state-space model identification class of algorithms, Int. J. Control 56 (5) (1992) 1211–1241. doi:10.1080/00207179208934363.

[7] M. Verhaegen, P. Dewilde, Subspace model identification, part 2. Analysis of the elementary output-error state-space model identification algorithm, Int. J. Control 56 (5) (1992) 1211–1241. doi:10.1080/00207179208934364.

[8] M. Verhaegen, Subspace model identification, part 3. Analysis of the ordinary output-error state-space model identification algorithm, Int. J. Control 58 (3) (1993) 555–586. doi:10.1080/00207179308923017.

[9] M. Verhaegen, Identification of the deterministic part of MIMO state space models given in innovations form from input-output data, Automatica 30 (1) (1994) 61–74. doi:10.1016/0005-1098(94)90229-1.

[10] P. Van Overschee, B. de Moor, N4SID: Numerical algorithms for state space subspace system identification, IFAC Proceedings Volumes 26 (2) (1993) 55–58. doi:10.1016/S1474-6670(17)48221-8.

[11] P. Van Overschee, B. De Moor, N4SID: Subspace algorithms for the identification of combined deterministic-stochastic systems, Automatica 30 (1) (1994) 75–93. doi:10.1016/0005-1098(94)90230-5.

[12] P. Van Overschee, B. De Moor, A unifying theorem for three subspace system identification algorithms, Automatica 31 (12) (1995) 1853–1864. doi:10.1016/0005-1098(95)00072-0.

[13] W. E. Larimore, Canonical variate analysis in identification, filtering, and adaptive control, in: 29th IEEE Conference on Decision and control, IEEE, IEEE, 1990, pp. 596–604. doi:10.1109/cdc.1990.203665.

[14] H. Akaike, Stochastic theory of minimal realization, IEEE Transactions on Automatic Control 19 (6) (1974) 667–674. doi:10.1109/tac.1974.1100707.

[15] H. Akaike, Markovian representation of stochastic processes by canonical variables, SIAM journal on control 13 (1) (1975) 162–173. doi:10.1137/0313010.

[16] H. Akaike, Canonical correlation analysis of time series and the use of an information criterion, Mathematics in science and engineering 126 (1976) 27–96. doi:10.1016/s0076-5392(08)60869-3.

[17] W. E. Larimore, Predictive inference, sufficiency, entropy and an asymptotic likelihood principle, Biometrika 70 (1) (1983) 175–181. doi:10.1093/biomet/70.1.175.

[18] H. Akaike, Information theory and an extension of the maximum likelihood principle, in: Second International Symposium on Information Theory, Akademia Kiadom, 1973, pp. 267–281. doi:10.1007/978-1-4612-0919-5_38.

[19] R. E. Kalman, A new approach to linear filtering and prediction problems, J. Basic Eng. 82 (1) (1960) 35–45. doi:10.1115/1.3662552.

[20] R. E. Kalman, R. S. Bucy, New results in linear filtering and prediction theory, J. Basic Eng. 83 (1) (1961) 95–108. doi:10.1115/1.3658902.

[21] L. N. Trefethen, Pseudospectra of matrices, in: Numerical Analysis 1991, Griffiths and Watson, Longman Scientific & Technical, Harlow, Essex UK, 1992, 1991, pp. 234–266.

[22] M. Embree, L. N. Trefethen, Spectra and Pseudospectra: The Behavior of Nonnormal Matrices and Operators, Princeton University Press, Princeton, 2005. doi:10.1515/9780691213101.

[23] C. Harris, et al., Array programming with NumPy, Nature 585 (7825) (2020) 357–362. doi:10.1038/s41586-020-2649-2.

[24] R. B. Lehoucq, D. C. Sorensen, C. Yang, ARPACK users' guide: solution of large-scale eigenvalue problems with implicitly restarted Arnoldi methods, SIAM, 1998. doi:10.1137/1.9780898719628.

[25] L. Carassale, M. Marrè-Brunenghi, S. Patrone, Wavelet-based identification of rotor blades in passage-through-resonance tests, Mechanical Systems and Signal Processing 98 (2018) 124–138. doi:10.1016/j.ymssp.2017.04.023.

[26] S. Mallat, A wavelet tour of signal processing, Elsevier, Boston, 1999.

## Appendix A. Proof of $\ker(L_{22}) \subset \ker(L_{32})$

A summary of the proof of $\ker(L_{22}) \subset \ker(L_{32})$ in [4, p. 164] is proposed here. Let $\nu$ column vector such as $L_{22}\nu = 0$. Then, right multiplying by the appropriate vector, equation (7) leads to the equations below.

$$\begin{bmatrix} U_f \\ Z_p \\ Y_f \end{bmatrix} \begin{bmatrix} Q_1^T & Q_2^T & Q_3^T \end{bmatrix} \begin{bmatrix} 0 \\ \nu \\ 0 \end{bmatrix} = \begin{bmatrix} L_{11} & 0 & 0 \\ L_{21} & L_{22} & 0 \\ L_{31} & L_{32} & L_{33} \end{bmatrix} \begin{bmatrix} 0 \\ \nu \\ 0 \end{bmatrix}$$

$$\begin{bmatrix} U_f \\ Z_p \\ Y_f \end{bmatrix} Q_2^T \nu = \begin{bmatrix} 0 \\ L_{22}\nu \\ L_{32}\nu \end{bmatrix}$$

As $\nu$ is taken such as $L_{22}\nu = 0$, the vector $L_{32}\nu$ is part of an input/output pair having past states null and future excitations null which implies, using the causality principle, all future observations are null, *i.e.* $L_{32}\nu = 0$.

## Appendix B. Optimal prediction

Equations (11) and (16) have been presented as the "projected" optimal prediction because they propose estimation for the optimal prediction $\zeta$ submitted to the projection operator $\Pi_{U_f}^{\perp}$. N4SID framework also proposes to estimate the optimal prediction $\zeta$ directly. Indeed, it is possible to have term to term identification in the identity relation given by equations (6) and (10).

$$V_f' = L_{33} Q_3 \tag{B1a}$$

$$\Psi_h U_f = \left(L_{31} - L_{32} L_{22}^{+} L_{21}\right) L_{11}^{-1} U_f \tag{B1b}$$

$$\zeta \coloneqq \mathcal{O}_h X_f = L_{32} L_{22}^{+} Z_p \tag{B1c}$$

*Optimal prediction* (`N4SID`)

The detailed demonstration of the above results uses assumptions (H1-3) and is available in references articles [11] and [4, p. 161].